Contrib Mineral Petrol (2007) 153:55–66
DOI 10.1007/s00410-006-0134-z

ORIGINAL PAPER

# Do carbonate liquids become denser than silicate liquids at pressure? Constraints from the fusion curve of $K_2CO_3$ to 3.2 GPa

**Qiong Liu · Travis J. Tenner · Rebecca A. Lange**

Received: 18 October 2005 / Accepted: 21 July 2006 / Published online: 14 September 2006

**Abstract** Brackets on the melting temperature of $K_2CO_3$ were experimentally determined at 1.86 ± 0.02 GPa (1,163–1,167°C), 2.79 ± 0.03 GPa (1,187–1,195°C), and 3.16 ± 0.04 GPa (1,183–1,189°C) in a piston-cylinder apparatus. These new data, in combination with published experiments at low pressure (<0.5 GPa), establish the $K_2CO_3$ fusion curve to 3.2 GPa. On the basis of these experiments and published thermodynamic data for crystalline and liquid $K_2CO_3$, the high-pressure density and compressibility of $K_2CO_3$ liquid were derived from the fusion curve. The pressure dependence of the liquid compressibility ($K'_0 = dK_0/dP$, where $K_0 = 1/\beta_0$) is between 16.2 and 11.6, with a best estimate of 13.7, in a third-order Birch–Murnaghan equation of state (EOS). This liquid $K'_0$ leads to a density of 2,175 ± 36 kg/m$^3$ at 4 GPa and 1,500°C, which is ~30% lower than that reported in the literature on the basis of the falling-sphere method at the same conditions. The uncertainty in the liquid $K'_0$ leads to an error in melt density of ± 2% at 4 GPa; the error decreases with decreasing pressure. With a $K'_0$ of 13.7, the compressibility of $K_2CO_3$ at 1,500°C and 1 bar ($K_0$ = 3.8 GPa) drops rapidly with increasing pressure ($K_{4\,\mathrm{GPa}} = 33$ GPa), which prevents a density crossover with silicate melts, such as $CaAlSi_2O_8$ and $CaMgSi_2O_6$, at upper mantle depths.

Communicated by I. Carmichael.

Q. Liu (✉) · T. J. Tenner · R. A. Lange
Department of Geological Sciences, University of Michigan,
1100 N. University Ave, Ann Arbor, MI 48109-1005, USA
e-mail: qiongl@umich.edu

## Introduction

An equation of state (EOS; *P–V–T* relation) for carbonate liquids is of considerable geological interest despite the fact that carbonate magmas are volumetrically sparse compared to silicate magmas. They are the first melts to form from upwelling carbonated mantle (e.g., Dalton and Presnall 1998; Dasgupta et al. 2004), and they are efficient agents of mantle metasomatism because of their high reactivity, high mobility, and high concentrations of incompatible trace elements (e.g., Green and Wallace 1988; Dalton and Wood 1993; Yaxley et al. 1998). Therefore, information on the density and compressibility of carbonate liquids to high pressure is required for an assessment of their buoyancy in the deep mantle, as well as their thermodynamic stability to high pressure.

Currently, the only high-pressure density data for carbonate liquids are those obtained by Dobson et al. (1996) with the falling-sphere method on three synthetic compositions ($K_2CO_3$, $KCa_{0.5}CO_3$, and a rare-earth element carbonate). Using Au and Pd spheres at 4 GPa, these authors report a density of 3,100 kg/m$^3$ for $K_2CO_3$ liquid at 1,500°C, which is remarkably dense and significant for two reasons. First, it suggests a density crossover between this liquid and its crystalline equivalent (Liu and Lange 2003), and thus a negative d*T*/d*P* fusion slope, at relatively low pressure (<1 GPa). Second, it indicates a density crossover with silicate melts at upper mantle pressures. For example, $CaAl_2Si_2O_8$ liquid and $CaMgSi_2O_6$ liquid have a density of 2,907 and 2,882 kg/m$^3$, respectively, at 4 GPa and 1,500°C (Rigden et al. 1989; Ai and Lange 2005) and are thus ~5–6% less dense than the reported value for $K_2CO_3$ liquid. In contrast, at 1 bar, these two silicate liquids are ~36% more dense than $K_2CO_3$ liquid (Lange 1997; Liu and Lange 2003). This unexpected density crossover between carbonate and silicate melt is plausible, however, because the 1 bar compressibility of $K_2CO_3$ liquid is 547 and 630% larger than those of the two silicate liquids (Zhu et al. 1991; Ai and Lange 2005). The results outlined above suggest that alkali carbonate liquids may be stable at low temperatures at upper mantle depths and may become denser than silicate melts near 4 GPa, which has implications for the migration of carbonate melts in the mantle, especially those rich in alkalis. Owing to the significance of these inferences, it is important to independently verify the reported density of high-pressure carbonate liquids obtained by the falling-sphere method.

To date, there are only four experimental techniques by which most high-pressure density data for liquids have been obtained: (1) shock-wave experiments (e.g., Rigden et al. 1989), (2) the sink/float approach (e.g., Agee and Walker 1993), (3) the falling-sphere method (e.g., Scarfe et al. 1979), and (4) fusion curve analysis (e.g., Lange 2003). Unfortunately, measuring the density of carbonate liquids at high pressure is not straightforward, especially for those rich in the alkaline-earth components. For example, shock-wave experiments are not yet feasible for $CaCO_3$ and $MgCO_3$ liquids, because they decompose at temperatures below their liquidus at 1 bar. To perform a shock-wave experiment on a liquid, the sample is first heated to temperatures above its liquidus at 1 bar (e.g., Rigden et al. 1989). The sink/float technique requires solid markers with well-known EOSs that will not react with the liquid. For carbonate liquids, there are few well-characterized crystalline markers that will both tightly bracket the density of these liquids and not react or dissolve. The falling-sphere method uses Stoke's Law to derive both viscosity and density of a liquid from the velocity of a falling sphere. However, as discussed in the section entitled the density of $K_2CO_3$ liquid with pressure, errors in melt density obtained by this technique are often >20%. The final method, fusion curve analysis, is the one most suitable for obtaining high-pressure density for alkali carbonate liquids (e.g., $Li_2CO_3$, $Na_2CO_3$, $K_2CO_3$; Liu and Lange 2003), although it cannot yet be applied to alkaline-earth carbonate liquids owing to their decomposition at 1 bar, which precludes calorimetric measurements of their heats of fusion.

Fusion curve analysis is a comparison between phase equilibrium experiments on the melting reaction of a mineral that melts congruently and the calculated melting reaction for that mineral obtained from measured thermodynamic properties. It thus tests whether a set of phase equilibrium experiments is consistent with an independent set of thermodynamic property measurements. Fusion curve analysis also has the potential to constrain the value of a single thermodynamic property for which direct, independent measurements are either difficult or not feasible. For example, the density of $K_2CO_3$ liquid at high pressures can be derived if high-quality, phase equilibrium experiments on its congruent melting reaction are obtained and all other requisite thermodynamic data are known. Currently, there are sufficient high-quality thermodynamic data to allow the fusion curve for $K_2CO_3$ to be calculated to 0.5 GPa (Liu and Lange 2003); at higher pressures it is necessary to include the pressure dependence of the liquid compressibility, which is currently unknown. In this study, we experimentally determined the fusion curve for $K_2CO_3$ between 1.9 and 3.2 GPa and compared the results with the calculated melting reaction to derive the density and compressibility of $K_2CO_3$ liquid as a function of pressure.

$K_2CO_3$ liquid was chosen for the study because it is not yet possible to measure the high-pressure density of a natural carbonatite liquid (i.e., one that is rich in the $MgCO_3$ and $CaCO_3$ components), except by the falling-sphere method, for the reasons outlined above. However, this technique leads to large errors in melt density (see discussion section below), whereas fusion curve analysis provides an opportunity to obtain the high-pressure density of the alkali carbonate liquids with significantly smaller errors (≤ 2%) at pressures up to 4 GPa. Of the three alkali (Li, Na, K) carbonates for which the best thermodynamic data are available, $K_2CO_3$ was chosen in order to directly test the results of Dobson et al. (1996) and the implied density crossover between carbonate and silicate liquids at upper mantle depths.

## Thermodynamic calculation of the fusion curve

The equation used to calculate crystal–liquid equilibrium for $K_2CO_3$ as a function of temperature and pressure is

$$\Delta H_{T_\mathrm{f}} + \int_{T_\mathrm{f}}^{T} \Delta C_P(T)\mathrm{d}T - T\left(\Delta S_{T_\mathrm{f}} + \int_{T_\mathrm{f}}^{T} \frac{\Delta C_P(T)}{T}\mathrm{d}T\right) = -\int_{1}^{P} \Delta V_T(P)\mathrm{d}P. \tag{1}$$

In Eq. 1, $T_\mathrm{f}$ is the 1 bar melting temperature of crystalline $K_2CO_3$, $\Delta H_{T_\mathrm{f}}$ and $\Delta S_{T_\mathrm{f}}$ the enthalpy and entropy of fusion at $T_f$, respectively, $\Delta C_P(T)$ the heat capacity of the liquid minus that of the crystal, $\Delta V_T(P)$ the volume of the liquid minus that of the crystal. A brief description of the thermodynamic data used in this study is given below.

## Thermodynamic data

### The 1 bar melting temperature ($T_f$)

The reported value for the 1 bar melting temperature ($T_f$) of $K_2CO_3$ varies over a 10° range in the literature. The JANAF thermochemical tables (4th edition; Chase 1998) list 1,174 K, based on the work of Reisman (1958). However, Janz et al. (1963) report lower temperatures of 1,171 and 1,169 K, respectively, in Tables 1 and 2 in their drop calorimetric study. Rolin and Recapet (1964) also give 1,171 K as the 1 bar melting temperature, but additionally present drop calorimetric data that show $K_2CO_3$ is liquid at 1,171 K. Finally, most chemical companies (e.g., Alfa-Aesar, J.T. Baker, etc.) report a value of 1,164 K on their chemical data sheets for high-purity $K_2CO_3$. To resolve which is the correct 1 bar melting temperature, we performed a series of experiments to bracket its value (described in the section entitled experiments at 1 bar); our results confirm that the 1 bar melting temperature for $K_2CO_3$ is 1,170 ± 2 K.

### The enthalpy and entropy of fusion

Both Janz et al. (1963) and Rolin and Recapet (1964) report a value for the enthalpy of fusion ($\Delta H_{T_f}$) of 27.6 ± 0.4 kJ/mol at 1,171 K, which is also recommended in the JANAF tables (Chase 1998). This value for $\Delta H_{T_f}$ is used in this study at a melting temperature of 1,170 K. The entropy of fusion ($\Delta S_{T_f} = 23.6\,\mathrm{J/mol\,K}$) is calculated from the relationship:

$$\Delta H_{T_f} - T_f \Delta S_{T_f} = 0. \tag{2}$$

An uncertainty of ± 0.4 kJ/mol in $\Delta H_{T_f}$ leads to an uncertainty in the calculated fusion temperature of ± 4° at 3 GPa.

The heat capacity of both crystalline and liquid $K_2CO_3$ must be known to permit integration in temperature (Eq. 1). Currently, there have not been any direct $C_P$ measurements on $K_2CO_3$ by differential scanning calorimetry. The best estimate for the liquid heat capacity is derived from the drop calorimetric data of Rolin and Recapet (1964) between 1,171 and 1,306 K, which leads to a value of 231 J/mol K (used in this study). In contrast, the enthalpy data of Janz et al. (1963) over a narrow temperature interval (< 70°) lead to a liquid heat capacity (209 J/mol K) that becomes less than that for the crystal above 1,200 K, which is unlikely. For the crystalline heat capacity, we use the values given in the JANAF tables, which are derived by differentiation of the enthalpy data from Janz et al. (1963). We fitted the values between 298 and 1,170 K to a form of the heat capacity equation (units are J/mol K) recommended by Berman and Brown (1985), which allows reliable extrapolation to high temperature:

$$C_P = 442.6 - 8,914T^{-0.5} + 34,278,267T^{-2} - 5,240,000,000T^{-3}. \tag{3}$$

An uncertainty in $\Delta C_P$ of ± 10 J/mol K leads to an uncertainty in the calculated fusion temperature of ± 12° at 3 GPa.

**Table 1** Experimental results for NaCl melting reaction

| Run # | Pressure (nominal) (GPa) | Hotspot temperature (°C) | Pt/Rh sphere position | Capsule length (mm) |
|---|---|---|---|---|
| A51 | 2.0 | 1,123 | Top | 3.78 |
| A55 | 2.0 | 1,131 | Top | 3.46 |
| A53 | 2.0 | 1,138 | Bottom | 3.68 |
| A49 | 2.0 | 1,146 | Bottom | 3.63 |
| A48 | 2.0 | 1,153 | Bottom | 3.50 |

**Table 2** Experimental results for $K_2CO_3$ melting reaction

| Run # | Pressure (calibrated) (GPa) | Hotspot temperature (°C) | Pt/Rh sphere position | Capsule length (mm) |
|---|---|---|---|---|
| A29 | 1.86 | 1,169 | Top | |
| A32 | 1.86 | 1,172 | Top | 2.69 |
| A31 | 1.86 | 1,174 | Bottom | 2.93 |
| A30 | 1.86 | 1,179 | Bottom | |
| A22 | 2.79 | 1,151 | Top | 3.65 |
| A23 | 2.79 | 1,191 | Top | |
| A27 | 2.79 | 1,196 | Top | 3.35 |
| A28 | 2.79 | 1,198 | Bottom | 2.10 |
| A21 | 2.79 | 1,201 | Bottom | 4.00 |
| A25 | 2.79 | 1,206 | Bottom | 2.75 |
| A26 | 2.79 | 1,211 | Bottom | 3.80 |
| A24 | 2.79 | 1,221 | Bottom | 3.02 |
| A20 | 2.79 | 1,301 | Bottom | 3.64 |
| A41 | 3.16 | 1,189 | Top | 2.49 |
| A42 | 3.16 | 1,192 | Top | 2.77 |
| A40 | 3.16 | 1,195 | Bottom | 2.77 |
| A39 | 3.16 | 1,198 | Bottom | 3.59 |
| A38 | 3.16 | 1,204 | Bottom | 2.49 |

## The volume, thermal expansion, and compressibility of $K_2CO_3$ crystal and liquid

The high-temperature crystalline phase is hexagonal $\alpha$-$K_2CO_3$. X-ray diffraction experiments by Schneider and Levin (1973) on $\alpha$-$K_2CO_3$ between 698 and 1,078 K lead to the following volume equation as a function of $T$ (K) at 1 bar:

$$V(T)^{\text{crystal}}_{K_2CO_3} = 64.248\ \exp(14.8 \times 10^{-5}(T - 1,078\,K))\ \text{cm}^3/\text{mol}. \tag{4}$$

The coefficient of thermal expansion, $\alpha_0 = 14.8 \times 10^{-5}\ \text{K}^{-1}$, is assumed in Eq. 4 to be independent of temperature. An uncertainty of ± 2% in $\alpha_0$ for crystalline $K_2CO_3$, with all other thermodynamic data unchanged, leads to an uncertainty of ± 8° in the calculated fusion temperature at 3 GPa.

Unfortunately, there are no experimental data on the compressibility of the crystalline alkali carbonates. However, S. Redfern (personal communication) has computed their compressibility using a static lattice simulation. The zero-pressure bulk moduli from his high-temperature simulations are 70, 60, and 45 GPa for $Li_2CO_3$, $Na_2CO_3$, and $K_2CO_3$, respectively. These values are derived for use in a Birch–Murnaghan EOS with a $K'_0$ value of 4, as discussed more fully below. In this study, a value of 45 GPa is used for the bulk modulus for crystalline $K_2CO_3$ at 1 bar. An uncertainty of ± 5% leads to an uncertainty in the fusion temperature of ± 10° at 3 GPa.

The molar volume of $K_2CO_3$ liquid as a function of temperature is obtained from the measurements of Liu and Lange (2003):

$$V(T)^{\text{liquid}}_{K_2CO_3} = 71.50 + 0.01640(T - 1,100\,K)\ \text{cm}^3/\text{mol}. \tag{5}$$

The error for this equation is ≤ 0.2%, which leads to a maximum uncertainty of ± 6° in the calculated fusion temperature at 3 GPa.

The sound speed of $K_2CO_3$ liquid has been measured by Zhu et al. (1991), which in conjunction with the density data of Liu and Lange (2003) can be used to obtain the 1 bar compressibility of this liquid as a function of temperature:

$$\beta(T)^{\text{liquid}}_{K_2CO_3} = 14.2 + 0.0059(T - 1,100\,K)\,10^{-6}\ \text{bars}^{-1}. \tag{6}$$

An uncertainty of ± 1% in Eq. 6 leads to an uncertainty of ± 11° in the fusion temperature at 3 GPa. In summary, a propagation of all the errors in the 1 bar thermodynamic data leads to a combined error of ± 51° in the calculated fusion temperature at 3 GPa.

## Extension to high pressure and the Birch–Murnaghan equation of state

In order to extend calculations of the $K_2CO_3$ fusion curve to pressures above 0.5 GPa, the density and compressibility of both crystalline and liquid $K_2CO_3$ must be known to high pressure. This requires incorporation of the pressure dependence of the liquid and crystal compressibility (bulk modulus) into the volume expression in Eq. 1. The third-order Birch–Murnaghan EOS, a truncated series expansion derived from finite strain theory of solids (Birch 1978), models the volume of silicate liquids to high pressure (tens of GPa) remarkably well (e.g., Stixrude and Bukowinski 1990). The third-order form is

$$P = \frac{3}{2}K_{T,0}\left(R^{7/3} - R^{5/3}\right)\left[1 - \frac{3}{4}\left(4 - K'_0\right)\left(R^{2/3} - 1\right)\right], \tag{7}$$

where $R = V_{T,0}/V_{T,P}$, with $V_{T,0}$ the volume at temperature $T$ and zero pressure (1 bar) and $V_{T,P}$ the volume at temperature $T$ and pressure $P$; $K_{T,0}$ the bulk modulus at zero pressure; and $K'_0$ the pressure dependence of the bulk modulus at zero pressure. With this equation, $K'$ is not constrained to be independent of pressure, and the implied value of $K''$ ($\mathrm{d}K'/\mathrm{d}P$) is given in Anderson (1995):

$$K'' = -\frac{1}{K_{T,0}}\left[(3 - K')(4 - K') + \frac{35}{9}\right]. \tag{8}$$

In the Birch–Murnaghan EOS, for $K'_0$ values less than 4, the pressure dependence to the compressibility changes sign with increasing pressure, which is not expected for most liquids. Therefore, in this study, for cases where $K'_0 < 4$, the Murnaghan EOS is used instead, where $K'$ is a constant with pressure:

$$V = V_0\left[1 + \frac{K'P}{K_0}\right]^{-1/K'}. \tag{9}$$

Incorporation of the Murnaghan relation (Eq. 9) into Eq. 1 is straightforward. However, incorporation of the Birch–Murnaghan relation (Eq. 7) into Eq. 1 requires a more complicated integration that is evaluated following a method suggested by P. Asimow (outlined in the Appendix of Ghiorso et al. 2002). The resultant integral is shown here:

$$\int_{1}^{P} V^{\mathrm{liq}}_{T,P}\mathrm{d}P = PV^{\mathrm{liq}}_{T,P} - V^{\mathrm{liq}}_{T,0} + \frac{9}{8}K_{T,0}V^{\mathrm{liq}}_{T,0}\left[R^{2/3}-1\right]^{2} \left\{1+\frac{1}{2}\left(K'_{0}-4\right)\left[R^{2/3}-1\right]\right\}. \qquad (10)$$

Utilization of Eq. 10 allows the temperature of the fusion curve to be calculated at high pressure for various $K'_0$ values for the liquid. In Fig. 1, a family of calculated fusion curves is shown for liquid $K'_0$ values that range from 4 to 18. Also shown are the differential thermal analysis (DTA) determinations of the fusion curve for $K_2CO_3$ to 0.45 GPa from Klement and Cohen (1975). The calculated fusion curve matches the DTA data within the propagated uncertainty of the thermodynamic data.

## Phase equilibrium experiments

A series of experiments were performed in a vertical tube furnace and in a 12.7 mm solid media piston-cylinder apparatus in order to bracket the temperature at which $K_2CO_3$ melts at 1 bar as well as at nominal pressures between 2 and 3.4 GPa. The strategy employed for this highly fluid liquid that does not quench to a glass is to place a small Pt–Rh bead on top of tightly packed crystalline $K_2CO_3$ powder, which is enclosed in a Pt capsule. The capsule is clearly and carefully marked to indicate the up direction. For those experiments in which melting occurs, the Pt–Rh bead will sink to the bottom of the capsule, whereas for those experiments where melting does not occur, the metal bead will be supported by the crystalline material underneath it. Because $K_2CO_3$ liquid has such a low viscosity and does not quench to a glass, a reversal on the melting reaction cannot be made. However, its low viscosity precludes problems with kinetics hindering the melting reaction, and it is expected that these experiments accurately locate the temperature of the melting reaction at the experimental pressures.

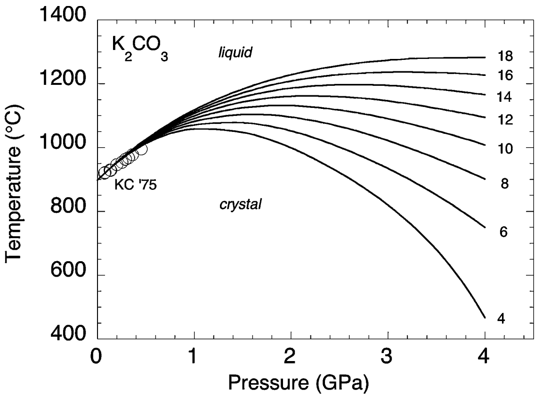

**Fig. 1** The $K_2CO_3$ fusion curve calculated from thermodynamic data to 4 GPa for various liquid $K'_0$ values (4–18) in a third-order Birch–Murnaghan EOS. The *open circles* are the experimentally determined melting temperatures with pressure from Klement and Cohen (1975)

### Experiments at 1 bar

Experiments at 1 bar were performed in a vertical tube furnace. The reagent grade (99.997% purity) $K_2CO_3$ powder was dried for several hours and compacted into Pt capsules of 5 mm diameter and 5 mm length. A Pt–Rh sphere was placed on top of the compacted powder, and the capsules were then suspended from a Pt cage in the hotspot of the furnace (< 1° thermal gradient). Temperature was measured with $Pt/Pt_{90}Rh_{10}$ (type S) thermocouple calibrated against the melting temperature of gold. The sample was held at 890°C for 1 h, and pulled out to examine whether the $K_2CO_3$ powder had melted or not. The sphere was still on top of the powder and thus melting did not occur at 890°C. This was repeated at 895°C (sphere on top; no melting) and 899°C (sphere sank; melting) and enabled a bracket to be placed between these two temperatures.

### Experiments at pressure

Experiments at nominal pressures of 2.0, 3.0, and 3.4 GPa were performed in a 12.7 mm piston-cylinder apparatus with cell assemblies that contained a $BaCO_3$ outer sleeve, a graphite furnace, and an inner MgO rod and tube (Fig. 2). The average capsule length was designed to be ~3 mm in length. Temperature was measured with $Pt/Pt_{90}Rh_{10}$ (type S) thermocouple, which has an error of ± 2°C over the temperature range

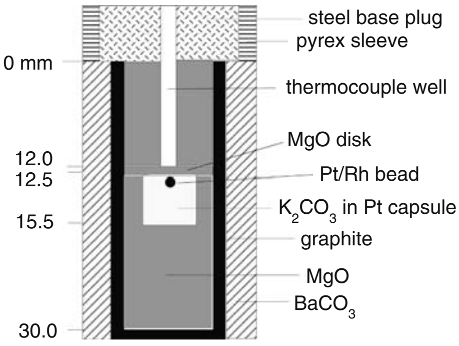

**Fig. 2** Schematic diagram of the pressure assembly in the piston-cylinder apparatus

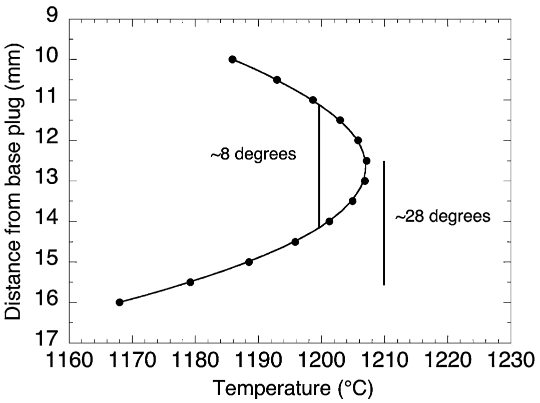

**Fig. 3** Experimentally determined thermal gradient in the pressure assembly as a function of distance from the base plug. When the hotspot is located in the center of a 3 mm capsule, the thermal gradient along the capsule length is ~8°C. When the hotspot is located at the top of the capsule, the thermal gradient is ~28°C

of the experiments. The location of the hotspot and the thermal gradient across the length of the sample capsule were mapped out at 2 GPa (nominal) through several experiments at different set points (300–1,400°C; Tenner 2005) where the temperatures of two thermocouples were measured: one in a fixed position to control the setpoint, whereas the other one was moved as a function of the distance from the base plug. The results are shown in Fig. 3 for a hotspot temperature of 1,207°C at 2 GPa. The measured thermal gradient allows a 3 mm long Pt capsule to be positioned so that when the hotspot is in the center, there is a gradient of only 8° along the capsule length. Alternatively, a 3 mm long capsule can be positioned so that the hotspot is at the top of the capsule, which gives rise to a thermal gradient of 28° along the capsule length, but also ensures a steadily declining temperature from top to bottom. This latter configuration was chosen for the experiments in this study in order to prevent thermal convection in the highly fluid $K_2CO_3$ liquid and to permit unambiguous interpretation of the quenched run products.

Pressure was monitored during all experiments with a 30.5 cm Heise gauge, which has a precision of ± 0.1% of the measured oil pressure. The pressure correction for the $BaCO_3$ cell used in this study was determined by bracketing the melting temperature of NaCl at a nominal pressure of 2 GPa, using the same strategy outlined above for $K_2CO_3$. The melting curve for NaCl is well documented to 1.8 GPa from DTA experiments of Clark (1959) in an internally heated gas pressure vessel as well as at 4.95 ± 0.20 GPa (1,457 ± 10°C) from experiments in a multi-anvil device using in situ X-ray radiography (Lange and Chen 2005). Bohlen (1984) additionally bracketed the NaCl melting reaction at 0.5 GPa in an internally heated pressure vessel. Lange and Chen (2005) used fusion curve analysis to calculate the NaCl melting curve from available thermodynamic data; their recommended curve matches all the experimental temperatures with an average deviation of ± 3° and a maximum deviation of 8°. This curve permits calculation of the NaCl melting temperature at any pressure between 0 and 5 GPa.

The results of our experiments on the melting reaction for reagent grade NaCl (99.997% purity) at a nominal pressure of 2 GPa are shown in Fig. 4, where the thermal gradient along the lengths of the capsules is also shown. The results indicate that the melting temperature is between 1,121 and 1,127°C (1,124 ± 3°C). This corresponds to a pressure of 1.86 ± 0.02 GPa for the NaCl melting curve, which indicates a pressure correction of – 7 ± 1%. For comparison, a – 9 ± 2% correction for $BaCO_3$ cells was reported by McDade et al. (2002) at Bristol University, and a – 6% correction for $BaCO_3$ cells was obtained at the University of Minnesota (M. Hirschmann, personal communication).

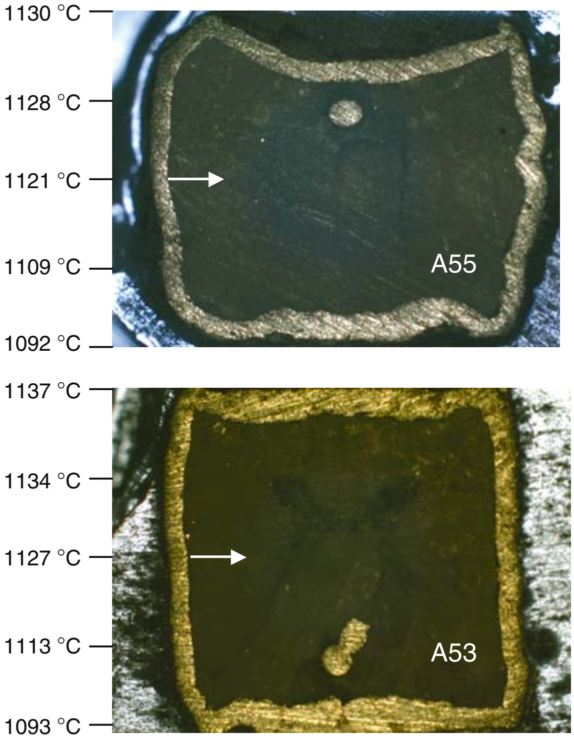

**Fig. 4** Reflected-light microphotographs of cut and polished charges for two experiments that bracket the NaCl melting reaction at a nominal pressure of 2 GPa. The orientation of the capsules is that during the experiments. The thermal gradient down the length of each capsule (Table 1) is shown. The *white arrows* indicate conservative estimates of the minimum (run A55) and maximum (run 53) melting temperature of NaCl

Therefore, our pressure correction is in agreement with those obtained at other laboratories.

For the experiments on the $K_2CO_3$ melting reaction, reagent grade (99.997% purity) $K_2CO_3$ powder was dried in an open Pt capsule (3 mm O.D.) at 400°C for at least 1 h before the capsule was sealed. A thin layer of $K_2CO_3$ powder was placed between the Pt/Rh bead and the top of the capsule to prevent the Pt/Rh bead from sticking to the top of the capsule. A thin (0.5 mm) MgO disk was placed above the capsule to prevent it from being punctured by the thermocouple ceramic during compression of the cell. The MgO in the assembly was heated at 400°C for ≥ 40 min prior to the experiments. To fix the position of the capsule, the MgO solid and MgO tube were set at 17.5 and 12 mm, with the 0.5 mm MgO disk in between, which added up to a total length of 30 mm (equal to the length of the graphite furnace). This placed the top of the capsule 12.5 mm below the base plug, at the location of the hotspot (Fig. 3). The samples were raised to the nominal pressure, held at room temperature for >1 hour before the temperature was ramped up to the target value. After the samples reached the target temperature, they were held for 40–50 min. During this interval, there was a slow increase in pressure, even though the oil supply was shut off and no leaking was visible in the system. In order to keep the pressure stable, the valve on the lower (master) ram was opened every time the pressure was 0.005 GPa above the desired value and the pressure was dropped to 0.005 GPa below the desired value. The valve was then left partially open to slow the pressure increase. This needed to be repeated five or six times over the course of each run. The exact same procedures were followed during the NaCl pressure calibration described above. Samples were quenched by shutting-off power to the graphite furnace. Capsule lengths in the various quenched run products (Table 2) varied from 2.10 to 3.35 mm (owing to different initial lengths of the capsules), which resulted in thermal gradients that ranged from 13° to 36° down the length of the capsules.

### Determination of negligible water contamination

An evaluation of possible contamination of our experiments by $H_2O$, which can diffuse from the surrounding furnace assembly materials, is critical because water may lower the melting temperature of $K_2CO_3$. Fortunately, it is not likely to have occurred for two reasons. First, furnace assemblies and the sample powder were thoroughly dried prior to each experiment. Second, several identical experiments of similar duration (~45 min) on $NaAlSi_3O_8$ glass (instead of $K_2CO_3$ powder) were performed by Tenner (2005) using the same procedures, the same pressure vessel, and over the same period of weeks as those reported in this study. The quenched glasses from the run products were subsequently analyzed for $H_2O$ by FTIR spectroscopy, and in all cases, they were found to contain less than 0.05 wt% $H_2O$ (Tenner 2005). These results confirm that the $BaCO_3$ and MgO components in the cell assembly were not a source of water contamination to the samples in the Pt capsules.

## Results

After each experiment, the capsules were dry polished to locate the Pt/Rh bead and to determine whether it sank to the bottom (melting occurred) or stayed on the top (no melting). Photomicrographs of the polished run products are shown in Fig. 5 for the pairs of experiments that bracket the melting temperature at each experimental pressure. The thermal gradient along the length of each capsule is also shown. The experimental results are presented in Table 2 and indicate that melting of $K_2CO_3$ occurs between 1,163 and 1,167°C at 1.86 ± 0.02 GPa, between 1,187 and 1,195°C at 2.79 ± 0.03 GPa, and between 1,183 and 1,189°C at 3.16 ± 0.04 GPa. The experimental results suggest that the $K_2CO_3$ fusion curve begins to flatten at ~2.5 GPa.

## Constraints on the $K'_0$ for $K_2CO_3$ liquid at high pressure

The experimental results that bracket the congruent melting reaction for $K_2CO_3$ are superimposed on a family of fusion curves calculated for different values of $K'_0$ (using the third-order Birch–Murnaghan EOS) for liquid $K_2CO_3$ in Fig. 6. The figure illustrates that the phase equilibrium experiments constrain the value for the liquid $K'_0$ to be ~13.7 ± 0.3. However, when the errors in the 1 bar thermodynamic data are considered, which lead to an uncertainty of ± 51° in the calculated fusion temperature at 3 GPa, the uncertainty in the liquid $K'_0$ value increases to +2.5 and − 2.1 units. Therefore, the best estimate for the liquid $K'_0$ is 13.7, with an upper and lower limit of 16.2 and 11.6, respectively.

## The density of $K_2CO_3$ liquid with pressure

Given a $K'_0$ value for $K_2CO_3$ liquid, its density can be calculated to high pressure using the Birch–Murnaghan

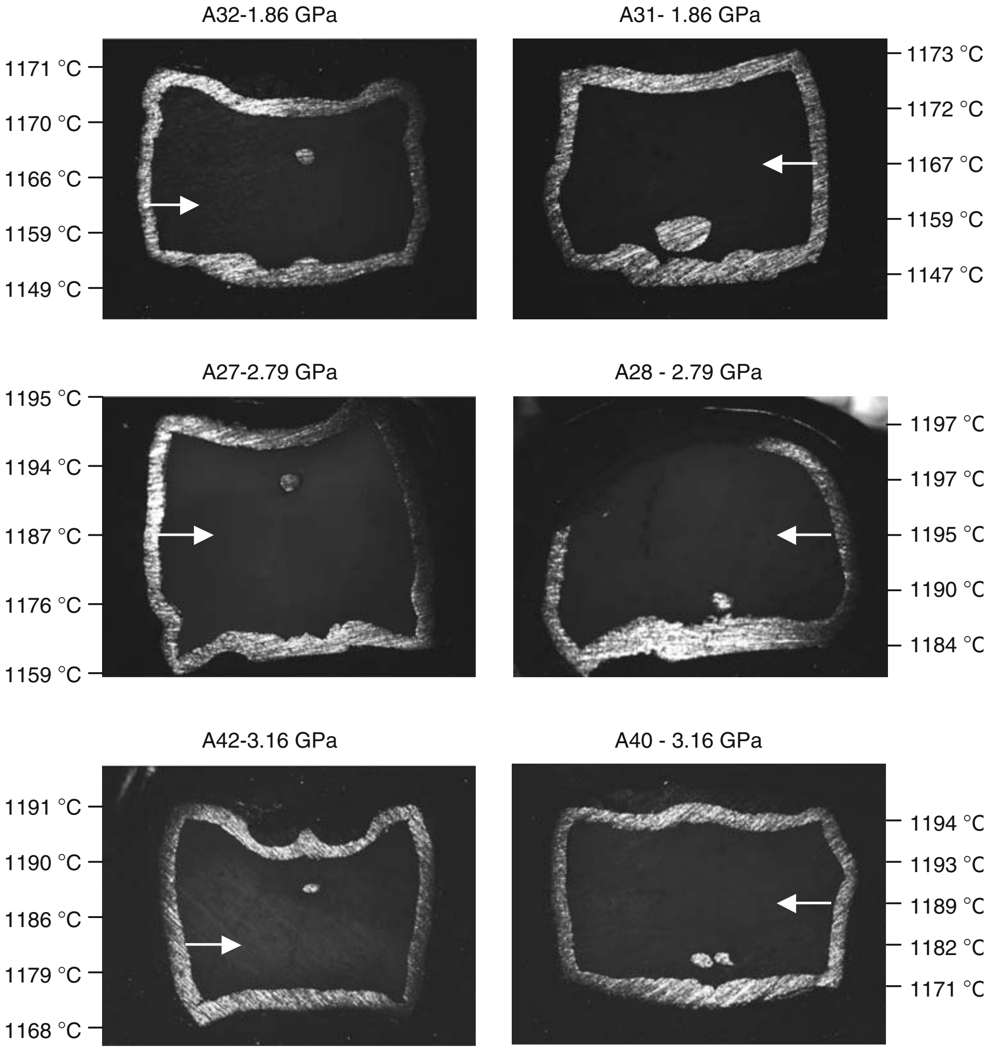

**Fig. 5** Reflected-light microphotographs of cut and polished charges for six experiments that bracket $K_2CO_3$ melting reaction at 1.86, 2.79, and 3.16 GPa. The orientation of the capsules is that during the experiments. The thermal gradient down the length of each capsule (Table 2) is shown. The *white arrows* indicate conservative estimates of the minimum (runs A32, A27, and A42) and maximum (runs A31, A28, and A40) melting temperatures of $K_2CO_3$

EOS (Eq. 7). The 1 bar density and bulk modulus for $K_2CO_3$ liquid used in this calculation are from Liu and Lange (2003) and Zhu et al. (1991). In Fig. 7, the density of $K_2CO_3$ liquid at 1,500°C is shown as a function of pressure for various liquid $K'_0$ values. The density versus pressure curve for a liquid $K'_0$ value of 13.7 is highlighted relative to those calculated for $K'_0$ values from 4 to 16.2. Also shown is the variation in the density of crystalline $K_2CO_3$. The results show that at 1,500°C, there is a density crossover between crystal and liquid at ~2.1 GPa. At 1,200°C, this crossover occurs at ~2.5 GPa, which is consistent with our experimental phase equilibrium results. The results also show that liquid $K_2CO_3$ remains strongly buoyant relative to silicate melts (e.g., $CaAlSi_2O_8$ and $CaMgSi_2O_6$) at 1,500°C and 4.0 GPa, with a density of 2,175 ± 36 kg/m$^3$ for a $K'_0$ value of 13.7 (+2.5 and – 2.1). This value is ~30% lower than the liquid density of 3,100 kg/m$^3$ reported by Dobson et al. (1996) at the same temperature and pressure.

In order to match the density given by Dobson et al. (1996), a $K'_0$ value less than 4 is required in the Birch–Murnaghan EOS. Therefore, the Murnaghan EOS (Eq. 9), with $K' = 1.6$, was used to obtain a density curve that intersects the density reported by Dobson et al. (1996) at 4 GPa (Fig. 7). The calculated fusion curve for this equation of state for $K_2CO_3$ liquid is shown in Fig. 6. For $K' = 1.6$, the calculated melting temperature is 441°C at 3.16 GPa and, therefore, ~750° lower than that experimentally determined in this study. Error analysis on the falling-sphere method reveals the cause of this discrepancy.

Dobson et al. (1996) employed an in situ X-ray shadowgraph technique in a multi-anvil apparatus to determine the density and viscosity of $K_2CO_3$ liquid using the falling-sphere method and the application of Stoke's Law:

$$v = \frac{2gr_s^2(\rho_s - \rho_l)}{9\eta_l}F, \tag{11}$$

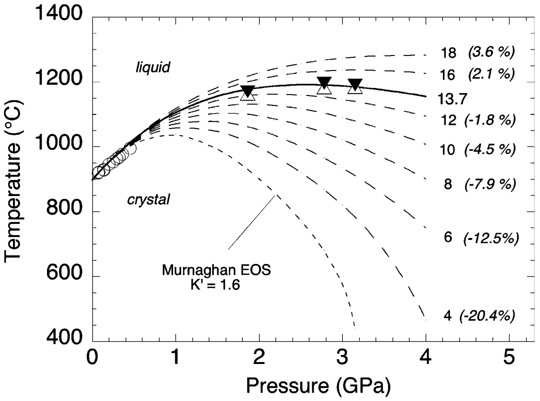

**Fig. 6** The calculated $K_2CO_3$ fusion curve for various liquid $K'_0$ values (4–18) in a third-order Birch–Murnaghan EOS. Also shown is the calculated fusion curve for a liquid $K'$ value of 1.6 in a Murnaghan EOS. The *open and solid triangles* represent the lowest and highest temperature brackets for each experimental pressure from the piston-cylinder runs. The *open circles* are the data of Klement and Cohen (1975). A liquid $K'_0 = 13.7$ leads to a calculated fusion curve that best matches the experimental brackets. For each fusion curve the deviation in melt density at 4 GPa (compared to that for a liquid $K'_0 = 13.7$) is shown in *parenthesis*

where $v$ and $r_s$ are the velocity and radius, respectively, of the falling sphere, $g$ the gravitational acceleration, $\rho_s$ and $\rho_l$ the density of the sphere and liquid, respectively, $\eta_l$ the liquid viscosity, and $F$ the third-order Faxen correction. Dobson et al. (1996) used Au and Pd spheres with a radius of 260 and 290 μm, respectively, to obtain melt density and viscosity. At 4 GPa and 1,500°C, Au and Pd have a density of ~18,530 and ~11,690 kg/m$^3$, respectively, both of which are considerably larger than the density of carbonate melts (<4,000 kg/m$^3$). Dobson et al. (1996) report velocities of 28 ± 0.73 mm/s (± 2.6%) and 17.5 ± 0.70 mm/s (± 4.0%) for the Au and Pd spheres, respectively, in their experiments. Despite the low relative errors on these velocity determinations, error analysis shows that these uncertainties in velocity alone lead to calculated melt density values that range between 1,666 and 4,256 kg/m$^3$; thus the reported melt density of 3,100 kg/m$^3$ has an error that exceeds ± 37%. This result shows that although the falling-sphere method provides an excellent measurement of melt viscosity (which varies over several orders of magnitude), it leads to errors that are unacceptably large for melt density. In contrast, the uncertainty in the $K'_0$ value of 13.7 of +2.5 and − 2.1 units, derived from fusion curve analysis, leads to an uncertainty in the density of liquid $K_2CO_3$ of ± 2% at 4 GPa; the error decreases with decreasing pressure. This result illustrates that fusion curve analysis can be an effective tool to obtain the density of high-pressure liquids.

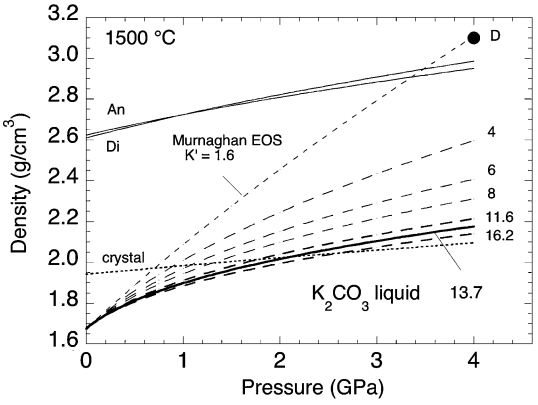

**Fig. 7** The density of $K_2CO_3$ liquid as a function of pressure at temperatures along the fusion curve. The curves are calculated with the 1 bar density and sound speed data of Liu and Lange (2003) and Zhu et al. (1991) and a third-order Birch–Murnaghan EOS. The *solid line* is for a liquid $K'_0 = 13.7$, whereas the *dashed lines* are for liquid $K'_0$ values of 4–16.2. Also shown is the calculated density for a liquid $K'$ of 1.6 in a Murnaghan EOS, which intersects the reported density of Dobson (*D*) at 4 GPa and leads to a density crossover with $CaAl_2Si_2O_8$ (*An*) and $CaMgSi_2O_6$ (*Di*) liquids. The *dotted line* is the density of crystalline $K_2CO_3$ as a function of pressure

## The compressibility of $K_2CO_3$ liquid with pressure

It is of interest to examine not only how the density of $K_2CO_3$ liquid varies with pressure for different $K'_0$ values (Fig. 7), but also how the compressibility changes. Its variation with pressure is calculated from the simple relation:

$$\beta_T(P) = \frac{1}{K_T(P)} = -\frac{1}{V_T}\left[\left(\frac{\partial P}{\partial V}\right)_T\right]^{-1}, \tag{12}$$

where $(\partial P/\partial V)_T$ is the derivative of the Birch–Murnaghan EOS (Eq. 7) with respect to volume (Lange 2003):

$$\begin{aligned}\left(\frac{\partial P}{\partial V}\right)_T = {} & \frac{3}{2}\frac{K_{T,0}}{V_{T,0}}\left(\frac{5}{3}R^{8/3} - \frac{7}{3}R^{10/3}\right) \\ & \left(1 - \frac{3}{4}(4 - K')\left(R^{2/3} - 1\right)\right) \\ & + \frac{3}{4}\frac{K_{T,0}}{V_{T,0}}\left(R^{7/3} - R^{5/3}\right)(4 - K')R^{5/3}.\end{aligned} \tag{13}$$

Equation 13 allows the compressibility of $K_2CO_3$ liquid to be calculated to high pressure for various $K'_0$ values. The resultant family of liquid compressibility curves at 1,500°C is shown in Fig. 8, along with that for crystalline $K_2CO_3$. There is a pronounced curvature in the liquid compressibility for a $K_0$ value of 13.7, with $\beta_T$ decreasing rapidly between 0 and 1 GPa and then less steeply at higher pressure. In contrast, a lower $K'_0$ value of 4 (commonly assumed for magmatic liquids) leads to a less sharp decrease in $\beta_T$ with pressure (Fig. 8). At 1 bar, there is a 12-fold increase in the compressibility of $K_2CO_3$ liquid relative to its crystalline equivalent, which rapidly diminishes to a 2-fold difference by 4 GPa. The enhanced compressibility of the liquid suggests that it compresses through a mechanism unavailable to the crystal, namely one that involves bond breaking.

The principle mechanism of compression for minerals (also available to liquids) involves continuous changes in either bond angles or bond lengths. Minerals may also undergo an abrupt phase transition to a higher-density structure with increasing pressure, which corresponds to an abrupt change in topology (e.g., calcite to aragonite). In contrast, liquids may undergo *continuous and gradual* changes in topology with increasing pressure, which requires bonds to be broken and reformed and thus reflects the dynamic character of liquids in contrast to solids. The continuous bond breaking that occurs in liquids has been directly observed through NMR spectroscopy (e.g., Stebbins 1995) and is seen in molecular dynamic simulations (e.g., Genge et al. 1995b).

There is strong evidence that carbonate liquids are topologically different from their crystalline equivalents. For example, in a Raman spectroscopic study on a synthetic carbonate (58 wt% $Na_2CO_3$, 21 wt% $CaCO_3$, 21 wt% $CaF_2$) at 1.6 GPa and ~700°C, Williams and Knittle (2004) found that the bonding of carbonate units is significantly altered when the crystalline material is melted and that at least two different varieties of carbonate groups are present in the liquid. Their results are consistent with spectroscopic evidence for two structurally distinct carbonate groups in $MgCO_3$–$K_2CO_3$ glasses at ambient pressure (Genge et al. 1995a). Williams and Knittle (2004) propose that the presence of at least two anionic bonding environments in carbonate liquids (undisrupted carbonate-like bonding similar to that found in crystalline carbonates and C–O bonding consistent with bridged cation–carbonate environments) leads to a wide range of structural configurations in the liquid. The enhanced compressibility of $K_2CO_3$ liquid at 1 bar, which is 1,190% greater than that for the crystal, reflects this wide range of configurations (and thus topologies) accessible to $K_2CO_3$ liquid through continuous bond breaking. What is notable, however, is that the high compressibility of the liquid at 1 bar is rapidly lost with increasing pressure (Fig. 8).

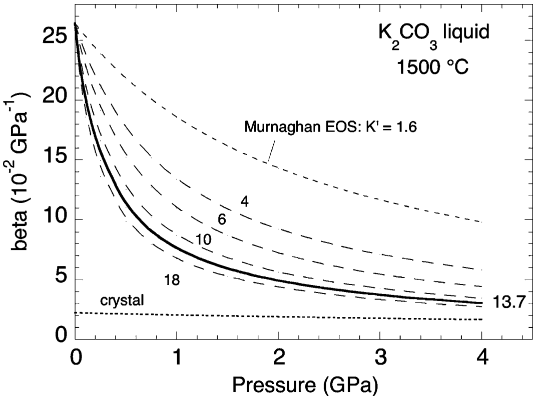

**Fig. 8** The isothermal compressibility ($\beta_T$) of $K_2CO_3$ liquid as a function of pressure at 1,500°C. The curves are calculated with the 1 bar density and sound speed data of Liu and Lange (2003) and Zhu et al. (1991) and a third-order Birch–Murnaghan EOS. The *solid line* is for a liquid $K'_0$ = 13.7, whereas the *dashed lines* are for liquid $K'_0$ values of 4–18. Also shown is the calculated compressibility for a liquid $K'$ of 1.6 in a Murnaghan EOS. The *dotted line* is $\beta_T$ for crystalline $K_2CO_3$

The degree to which the compressibility ($\beta_T$) of liquid $K_2CO_3$ drops with pressure can be compared to that for various silicate liquids. Figure 9 illustrates the relationship between $\beta_T$ and pressure for three different liquids: $K_2CO_3$, $CaAl_2Si_2O_8$, and $CaMgSi_2O_6$. The variations in $\beta_T(P)$ for $CaAl_2Si_2O_8$ and $CaMgSi_2O_6$ liquids are well known from shock-wave measurements (Rigden et al. 1989). The calculations for $\beta_T(P)$ are extended to 10 GPa, although this is an extrapolation of our experimental constraints to 3.2 GPa. Nonetheless, the comparison among the three diverse liquids is striking.

At 1,500°C, $K_2CO_3$ liquid has a large 1 bar value for $\beta_{T,0}$ of $\sim 26.4 \times 10^{-2}$ $GPa^{-1}$ ($K_0$ = 3.8 GPa), whereas it is ~4.82 and $4.19 \times 10^{-2}$ $GPa^{-1}$ for liquid $CaAl_2Si_2O_8$ and $CaMgSi_2O_6$ ($K_0$ = 20.7 and 23.9 GPa), respectively (Fig. 8). Because of the relatively large $K'_0$ value (13.7), $\beta_T(P)$ drops sharply between 0 and 1 GPa for $K_2CO_3$ liquid. By 3 GPa, $\beta_T$ is only ~14% of its 1 bar value, whereas $\beta_T$ is ~58% of the 1 bar values for both $CaAl_2Si_2O_8$ and $CaMgSi_2O_6$ liquids at this same pressure. Perhaps the most surprising feature is that the compressibility curves for all three liquids converge to similar values by 10 GPa and 1,500°C (~1.5 vs. ~1.5 vs. $\sim 1.3 \times 10^{-2}$ $GPa^{-1}$), which translates to liquid bulk moduli of ~66, 67, and 78 GPa, respectively, for $K_2CO_3$, $CaAl_2Si_2O_8$, and $CaMgSi_2O_6$. Therefore, the large variation in liquid compressibility for melts of vastly different composition is a *low-pressure* phenomenon, which likely arises from the wide variety of different topological mechanisms for compression that are accessible to these diverse liquids at low pressure.

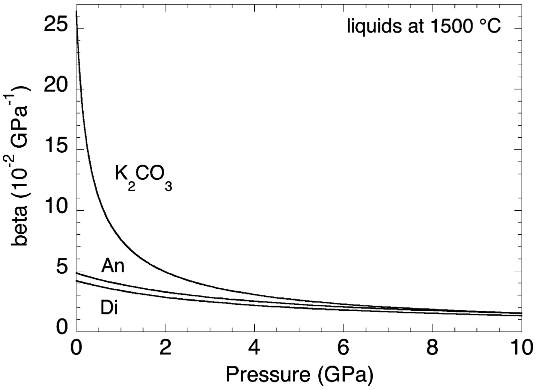

**Fig. 9** A comparison of the isothermal compressibility ($\beta_T$) variation with pressure for $K_2CO_3$, $CaAl_2Si_2O_8$ (An), and $CaMgSi_2O_6$ (Di) liquid at 1,500°C. The curve for $K_2CO_3$ liquid is calculated for $K'_0 = 13.7$

The relationship between the three compressibility curves in Fig. 9 illustrates why there is no density crossover between $K_2CO_3$ liquid and silicate liquids, such as $CaAl_2Si_2O_8$ and $CaMgSi_2O_6$, at upper mantle depths (e.g., Fig. 7). The remarkably large compressibility of $K_2CO_3$ liquid at 1 bar is lost too rapidly with increasing pressure to permit the density crossover with silicate liquids. This result is broadly consistent with the observation reported by Mattey et al. (1990) of a calcium-rich carbonate liquid floating on a sodium-rich silicate melt at 3 GPa. Nonetheless, additional work is required to confirm that naturally occurring carbonate melts remain buoyant relative to silicate (basaltic) melts throughout the upper mantle (≤ 14 GPa). In the meantime, this study has provided the first tight constraints on the density and compressibility of a carbonate liquid to high pressure.

**Acknowledgments** This research was supported by the National Science Foundation (EAR-0310079). Constructive reviews by Ian Carmichael, Don Baker, and Don Snyder significantly improved the manuscript.

## References

Agee CB, Walker D (1993) Olivine flotation in mantle melt. Earth Planet Sci Lett 114:315–324

Ai Y, Lange RA (2005) Sound velocity measurements of CaO–MgO–$Al_2O_3$–$SiO_2$ liquids: reevaluation of the equation of state for $CaMgSi_2O_6$–$CaAl_2Si_2O_8$ liquids. American Geophysical Union, EOS Transactions, Fall meeting supplement, Abstract MR13A-0063

Anderson OL (1995) Equation of state of solids for geophysics and ceramic science. Oxford University Press, New York, 405 pp

Berman RG, Brown TH (1985) The heat capacity of minerals in the system $K_2O$–$Na_2O$–CaO–MgO–FeO–$Fe_2O_3$–$Al_2O_3$–$SiO_2$–$TiO_2$–$H_2O$–$CO_2$: representation, estimation, and high temperature extrapolation. Contrib Mineral Petrol 89:168–183

Birch F (1978) Finite strain isotherm and velocities for single-crystal and polycrystalline NaCl at high-pressures and 300-degree-K. J Geophys Res 83:1257–1268

Bohlen SR (1984) Equilibria for precise pressure calibration and a frictionless furnace assembly for the piston-cylinder apparatus. N Jahrb Mineral Mon 9:404–412

Chase MW (1998) NIST-JANAF thermochemical tables, fourth edition. J Phys Chem Ref Data Monogr 9:621–623

Clark SP (1959) Effect of pressure on the melting points of eight alkali halides. J Chem Phys 31:1526–1531

Dalton JA, Presnall DC (1998) Carbonatitic melts along the solidus of model lherzolite in the system CaO–MgO–$Al_2O_3$–$SiO_2$–$CO_2$ from 3 to 7 GPa. Contrib Mineral Petrol 131:123–135

Dalton JA, Wood BJ (1993) The compositions of primary carbonate melt and their evolution through wallrock reaction in the mantle. Earth Planet Sci Lett 119:511–525

Dasgupta R, Hirschmann MM, Withers AC (2004) Deep global cycling of carbon constrained by the solidus of anhydrous, carbonated eclogite under upper mantle conditions. Earth Planet Sci Lett 227:73–85

Dobson DP, Jones AP, Rabe R, Sekine T, Kurita K, Taniguchi T, Kondo T, Kato T, Shimomura O, Urakawa S (1996) In-situ measurement of viscosity and density of carbonate melts at high pressure. Earth Planet Sci Lett 143:207–215

Genge MJ, Jones AP, Price GD (1995a) An infrared and Raman study of carbonate glasses: implications for the structure of carbonatite magmas. Geochim Cosmochim Acta 59:927–937

Genge MJ, Price GD, Jones AP (1995b) Molecular dynamics simulations of $CaCO_3$ melts to mantle pressures and temperatures: implications for carbonatite magmas. Earth Planet Sci Lett 131:225–238

Ghiorso MS, Hirschmann MM, Reiners PW, Kress VC (2002) pMelts: a revision of MLETS for improved calculation of phase relations and major element partitioning related to partial melting of the mantle to 3 GPa. Geochem Geophys Geosyst 3, 2001GC000217

Green DH, Wallace ME (1988) Mantle metasomatism by ephemeral carbonatite melts. Nature 336:459–462

Janz GI, Neuenschwander E, Kelly FJ (1963) High-temperature heat content and related properties for $Li_2CO_3$, $Na_2CO_3$, $K_2CO_3$, and the ternary eutectic mixture. Trans Faraday Soc 59:841

Klement W, Cohen LH (1975) Solid–solid and solid–liquid transitions in $K_2CO_3$, $Na_2CO_3$ and $Li_2CO_3$—investigations to greater than – 5 kbar by differential thermal-analysis—thermodynamics and structural correlations. Ber Bunsenges 79:327–334

Lange RA (1997) A revised model for the density and thermal expansivity of K2O-Na2O-CaO-MgO-Al2O3-SiO2 liquids between 701 and 1896 K: extension to crustal magmatic temperatures. Contrib Mineral Petrol 130:1–11

Lange RA (2003) The fusion curve of albite revisited and the compressibility of $NaAlSi_3O_8$ liquid with pressure. Am Mineral 88:109–120

Lange RA, Chen J (2005) The NaCl fusion curve: new experiments to 5 GPa and constraints on the liquid equation of state. American Geophysical Union, Transactions, Fall meeting, Abstracts MR13A-0064

Liu Q, Lange RA (2003) New density measurements on carbonate liquids and the partial molar volume of the $CaCO_3$ component. Contrib Mineral Petrol 146:370–381

Mattey DP, Taylor WR, Green DH, Pillinger CT (1990) Carbon isotopic fractionation between $CO_2$ vapour, silicate and carbonate melts: an experimental study to 30 kbar. Contrib Mineral Petrol 104:492–505

McDade P, Wood BJ, Van Westrenen W, Brooker R, Gudmundsson G, Soulard H, Najorka J, Blundy J (2002) Pressure corrections for a selection of piston-cylinder cell assemblies. Mineral Mag 66:1021–1028

Reisman A (1958) Reactions of the group VB pentoxides with alkali oxides and carbonates. IX. A DTA study of alkali metal carbonates. J Am Chem Soc 80:3558–3561

Rigden SM, Ahrens TJ, Stolper EM (1989) High-pressure equation of state of molten anorthite and diopside. J Geophys Res 94:9508–9522

Rolin M, Recapet JM (1964) Contribution a l'étude des proprietes thermódynamiques des carbonates alcalins. III. Courbes d'enthalpies en fonction de la température et chaleurs de fusion de $Na_2CO_3$, $Li_2CO_3$, $K_2CO_3$ et de leur mélange eutectique ternaire. Bull Soc Chim Fr 10:2504–2510

Scarfe CM, Mysen BO, Virgo D (1979) Changes in viscosity and density of melts of sodium disilicate, sodium metasilicate, and diopside composition with pressure. Carnegie Inst Wash Yearb 78:547–551

Schneider SJ, Levin EM (1973) Polymorphism of $K_2CO_3$. J Am Ceram Soc 56:218–219

Stebbins JF (1995) Dynamics and structure of silicate and oxide melts: nuclear magnetic resonance studies. In: Stebbins JF, McMillan PF, Dingwell DB (eds) Structure, dynamics and properties of silicate melts. Rev Mineral 32:191–246. Mineralogical Society of America, USA

Stixrude L, Bukowinski MST (1990) Fundamental thermodynamic relations and silicate melting with implications for the constitution of D″. J Geophys Res 95:19311–19325

Tenner TJ (2005) The albite fusion curve re-examined: new experiments and the density and compressibility of $NaAlSi_3O_8$ with pressure. Masters thesis, University of Michigan

Williams Q, Knittle E (2004) Structural complexity in carbonate liquid at high pressures. Geophys Res Lett 30:1022. DOI 10.1029/2001/GL013876

Yaxley GM, Green DH, Kamenetsky V (1998) Carbonatite metasomatism in the southern Australian lithosphere. J Petrol 39:1917–1930

Zhu H, Saito T, Sato Y, Yamamura T, Shimakage K, Ejima T (1991) Ultrasonic velocity and absorption coefficient in molten alkali metal nitrates and carbonates. J Jpn Inst Metals 55:937–944